Vol. 46, No. 4 (2024) 677-694, DOI: 10.24874/ti.1730.08.24.10

Tribology in Industry

www.tribology.rs

RESEARCH

Evaluation of the Tribological and Corrosion Resistance Properties of 24-Bilayer TiN/TiAlN Coatings in Simulated Body Fluid

Willian Arnulfo Aperador Chaparro[a,*], Julio Cesar Caicedo Angulo[b], Jorge Bautista-Ruiz[c]

[a]*Ingeniería Mecatrónica, Universidad Militar Nueva Granada, Bogotá, Colombia,*
[b]*Thin Films Group Universidad del Valle, Ciudad Universitaria Meléndez, A.A. 25360, Cali, Colombia*
[c]*Centro de Investigación en Materiales Cerámicos, Universidad Francisco de Paula Santander, 540003, San José de Cúcuta, Colombia,*

Keywords:

Tribocorrosion
Coatings [TiN/TiAlN]
Biocompatible Materials
Roughness

* Corresponding author:

Willian Arnulfo Aperador Chaparro
E-mail:
william.aperador@unimilitar.edu.co

Received: 12 August 2024
Revised: 12 September 2024
Accepted: 28 October 2024

A B S T R A C T

The tribocorrosive behavior of [TiN/TiAlN] coatings, consisting of 24 bilayers with a bilayer period (Λ) of 125 nm, was evaluated. There is a lack of studies on the tribocorrosion of TiN/TiAlN multilayer coatings applied to metallic prostheses. These coatings were obtained using a reactive RF magnetron sputtering system and deposited onto a Ti6Al4V alloy. This study represents the first evaluation of the tribocorrosive behavior of these coatings in simulated physiological environments. Various characterization techniques were employed, including X-ray diffraction (XRD), scanning electron microscopy (SEM), atomic force microscopy (AFM), pin-on-disk testing, electrochemical impedance spectroscopy (EIS), and Tafel curves. The coatings exhibited a face-centered cubic (FCC) structure, characterized by a partial arrangement of Ti and Al atoms. The research is motivated by the need for tribocorrosion-resistant coatings to enhance the durability of metallic prostheses. The results demonstrated a friction coefficient of 0.053 and a corrosion rate of 0.025 μm/year, highlighting the effectiveness of the coating. Changes in roughness were observed; however, no significant alterations in its formation were noted.

© 2024 Published by Faculty of Engineering

1. INTRODUCTION

Stainless steel 316 LVM has been studied due to its broad applicability, ranging from industrial to biomedical applications [1]. However, it has been determined that titanium and its alloys represent innovative materials in this field, offering significant advantages such as improved biocompatibility and excellent mechanical properties [2]. Precisely, the Ti6Al4V alloy is progressively displacing stainless steels in various biomedical applications. This shift is attributed to its superior biocompatibility, lower density, higher fatigue resistance, and lower elastic modulus than stainless steel [3]. These characteristics make Ti6Al4V a more suitable option for bone, dental,

and joint implants, significantly reducing the risk of adverse reactions, decreasing implant weight, mitigating fatigue from loading cycles, and minimizing stiffness differences with the surrounding bone tissue [4]. Despite being the most widely used titanium alloy in implants, studies indicate that, for permanent implant applications, it may present toxic effects due to the release of vanadium and aluminum [5]. For this reason, focused research has been conducted on critical properties responsible for biocompatibility, such as low electronic conductivity, high corrosion resistance, and thermodynamic state under physiological pH conditions.

Nanometric coatings have been developed through advanced technologies, with physical vapor deposition (PVD) and chemical vapor deposition (CVD) standing out among them [6]. Recently, a detailed review of these techniques can be found in the article by A. Baptista et al. [7], which provides a comprehensive overview of the current advancements and applications of PVD and CVD. These techniques enable the controlled application of materials at the nanoscale, providing unique and enhanced properties compared to conventional coatings [8]. PVD involves evaporating material from a solid target and depositing it onto the substrate to form a coating. In contrast, CVD relies on the chemical reaction of precursor gases on the substrate's surface, leading to material deposition in the form of a thin film. Nanotechnologies offer advantages such as increased homogeneity, precise control of coating thickness, and improved properties, making them suitable for various applications, from electronics to medicine [9].

Additionally, scientific research interest in the biocompatible properties of these materials has seen a significant rise in recent years [10]. This growth is attributed to their intriguing behavior in physical, chemical, and mechanical properties. To thoroughly understand the behavior of these coatings, especially concerning corrosion resistance, mechanical strength, and their ability to withstand corrosive agents, it is crucial to study their performance in simulated biological fluids (such as Hank's solution) and evaluate aspects like hemocompatibility, cytotoxicity, genotoxicity, among others, as these characteristics become crucial in various biocompatible applications [11]. Applying coatings on components made from biocompatible materials emerges as a viable modification to extend their lifespan to improve various properties, such as physical, mechanical, thermal, tribological, or chemical [12]. This process mainly aims to strengthen corrosion and wear resistance while promoting cell adhesion and stimulating osteointegration in biomedical implants [13]. The compelling need to coat biomaterials is grounded in the absence of a singular material that comprehensively meets all the rigorous requirements mentioned.

Coatings can optimize tribological properties, such as friction and lubrication, making the alloy more suitable for specific applications like mechanical components. Research has focused on studying and enhancing the properties of certain ceramics, including nitrides, carbides, and oxides, among others. TiN is a commonly used binary compound due to its mechanical and tribological properties, which significantly improve the performance of tools and components [14]. For this reason, researchers have continued to work on developing these coatings by introducing one or more elements to investigate the possibility of obtaining materials with multicomponent or multilayer structures with improved properties [15]. A recent approach in the development of TiN coatings involves the implementation of TiN/Ti multilayer structures. Sheng et al. [16] provides a comprehensive insight into how the number of layers in TiN/Ti coatings affects their microstructure, mechanical properties, and wear behavior. The authors fabricated TiN/Ti coatings with different layer numbers using high-power reactive magnetron sputtering. Their research revealed that increasing the number of layers refines the grains and transforms the preferred crystallographic orientation of TiN. Additionally, they found that the elastic modulus and hardness of the TiN/Ti coatings initially increase and then decrease with the number of layers. The two- and four-layer coatings exhibited the maximum elastic modulus and hardness, respectively. It was also observed that the layer number influences the adhesion and friction coefficient during wear tests, with the eight- and twelve-layer coatings showing higher wear rates compared to coatings with fewer layers. It has been reported that adding Al to the TiN coating results in higher hardness values (31.5 GPa), better thermal stability up to 850 °C, improved tribological behaviors, and enhanced electrochemical corrosion resistance compared to the binary nitride [17].These outcomes are attributed to the material's structural

characteristics, microstructure densification, covalent bonds, and the formation of dense films when subjected to extreme environments with elevated temperatures and corrosive agents.

Before using materials in implants, it is crucial to subject them to evaluations in a simulated physiological medium [18]. This medium, an electrolyte with chloride ions and a pH of approximately 7.4, can vary under specific conditions in the human body, being alkaline during infections and acidic in the presence of wounds and hematomas, respectively [19]. Research on the corrosion rate in titanium alloys has gained importance recently. Modular joints face deterioration due to friction corrosion in synovial fluids, a phenomenon linked to relative displacement or vibration. In orthopedic implants, micromovements occur at the fixation points. Friction corrosion, associated with relative displacement, involves material-tissue interaction, reaction to material degradation, tribological properties, and more [7][20]. The nature of the biomaterial is decisive for its introduction into the organism, as body fluids trigger biological responses that affect its performance [21]. These biomaterials must meet specifications, adapt to the organism, and have good elastic modulus, corrosion resistance, and fatigue life according to fatigue strength, as they are considered foreign bodies when exposed to body fluids, such as saliva and buffer solutions, titanium alloys react, releasing charge-free dissolved species due to their thin oxide layer, which can induce undesired biochemical reactions, such as protein deployment.

The coatings [TiN/TiAlN], consisting of 24 bilayers and applied on the Ti6Al4V alloy through a reactive r.f magnetron sputtering system, exhibit effective performance against tribocorrosion [22] [23]. When subjected to evaluation in an electrochemical cell integrated into a tribometer, these coatings demonstrated improved resistance to friction corrosion under simulated physiological media conditions. The various characterization techniques employed revealed beneficial structural and morphological properties, with minimal changes in roughness and asperities. Combined with the homogeneous, dense, and nanostructured formation achieved through the deposition method, these properties position the coatings as suitable biocompatible materials for metallic implants.

2. EXPERIMENTAL DETAILS

2.1 Coating deposition

The [TiN/TiAlN] multilayer coatings, consisting of 24 bilayers, were deposited onto Ti6Al4V substrates using a multi-target magnetron sputtering system with a radiofrequency (RF) source operating at 13.56 MHz. The system employed two stoichiometric metallic targets of Al and Ti, each with a purity of 99.9%. The optimized deposition parameters were as follows: sputtering power of 350 W for the Al targets and 400 W for the Ti targets. This power configuration was chosen to balance the deposition rate and film uniformity, considering the different sputtering yields of Al and Ti, which can cause slight non-homogeneity in layer thickness. The substrate was maintained at a temperature of 300°C and rotated at 60 RPM to facilitate the formation of stoichiometric coatings. The sputtering gas mixture consisted of 93% Ar and 7% N_2, with a total working pressure of 0.6 Pa (or 6 x 10^{-3} mbar) and a nitrogen gas flow of 3.7 sccm, which was kept constant to analyze the substitution effect when Al ions replace Ti atoms. An unbalanced RF bias voltage of -70 V was applied to enhance film quality and adhesion. The magnetron sputtering system was configured to deposit a fixed number of 24 bilayers with a bilayer period (Λ) of 150 nm.

Furthermore, the magnetron sputtering system featured a substrate positioning system associated with the target point, enabling the optimal number of bilayers, in this case, 24, to be obtained. This choice was based on previous research demonstrating that both the number of bilayers (24) and the reduction of bilayer period (125 nm) in nanometric multilayer coatings contribute to improving corrosion resistance, even under lower voltages [24].

2.2 Coating characterization

The crystallographic analysis of the coatings was performed using a Panalytical X-ray diffractometer with Cu-Kα radiation (wavelength λ = 1.5405 Å), operating at 45 kV and 40 mA. A parallel beam optical system was implemented, comprising a parabolic mirror in the incident beam, a 0.18° parallel plate collimator, and a flat graphite monochromator in the diffracted beam. X-ray scanning was conducted in the 5 to 90 degrees 2θ range, in step scanning mode with increments of 0.03° (2θ) and a counting time of 2 s.

The chemical composition of the coatings was analyzed using energy dispersive X-ray spectroscopy (EDX) with a Philips XL 30 FEG scanning electron microscope, which was equipped with a high-purity germanium (Ge) EDX detector to ensure accurate spectrum acquisition. The structural characteristics of the multilayers were examined by scanning electron microscopy (SEM) using the same Philips XL 30 FEG system, which featured a light optical magnification range from 525X to 24,000X and a height sensitivity backscatter electron detector (EDAX-EDX) for detailed imaging.

To determine the adhesion of the coating, the scratch test was performed using a Rockwell C indenter (conical with a 120° apex angle and 200 μm tip radius). The test involves moving the indenter across the sample while maintaining contact, either at a constant load or progressively increasing the load along the same scratch. The applied load (LW) increases until substrate deformation generates stress that lead to coating failure. The critical load (Lc), at which adhesive or cohesive failure occurs, was determined through friction coefficient measurements.

2.3 Preparation of fluid and bone pin

To prepare the simulated biological fluid, specific steps were meticulously followed. Firstly, the solution maintained a clear or transparent colour, and a plastic container without cracks or scratches was used [25]. The temperature of the distilled and deionized water was adjusted to 36.5°C.

Subsequently, the reagents were dissolved following the order specified in the table (table 1).

Table 1. Composition of the Solution for Experimental [26].

Reagent	Quantity
Distilled water	750 ml
NaCl	7.996 g
$NaHCO_3$	0.350 g
KCl	0.224 g
$K_2 HPO_4 * 3H_2 O$	0.228 g
$MgCl_2 * 6H_2O$	0.305 g
1 kmol/m³ HCl	40 cm³
$CaCl_2$	0.278 g
$Na_2 SO_4$	0.071 g
$(CH_2 OH)_3 CNH$	6.057 g
1 kmol/m³	Appropriate amount for
	pH adjustment

It was crucial to add the reagents $(CH_2 OH)_3 CNH$ 6.057 g and 1kmol/m³ in small quantities to adjust the pH while the HCl reagent was gradually incorporated. The volume was maintained by adding distilled and deionized water, considering a temperature of 36.5°C.

Before adding Tris (hydroxymethyl aminomethane), the pH was verified to be between 2±1.0. Tris was added gradually, ensuring it was completely dissolved before each addition. The pH was adjusted to 7.3±0.05, and the temperature was set to 36.5±0.5°C.

Tris was then added until a pH of 7.45 was reached. Subsequently, HCl 1kmol/m³ adjusted the pH to 7.42, ensuring it did not decrease below 7.40. This process was repeated until the Tris was exhausted, maintaining the pH between 7.42 and 7.45.

The temperature was adjusted to 36.5±0.2°C, and the pH was set to 7.42 with HCl 1kmol/m³, reaching a pH of 7.40. Finally, the volume was completed to 1000 ml with distilled and deionized water. The fluid was allowed to cool to 20°C, and it was transferred to a sealed container for storage at 10.5°C. Notably, the prepared fluid's shelf life was a maximum of 30 days [27-28].

Preparing an animal bone ball used as a counterpart in the tribometer involved selecting a bovine metacarpal diaphysis and making a precise cut with a bone saw. Subsequently, the surface was conditioned with a file, and a central hole was drilled to simulate the medullary cavity. After cleaning any bone residue, the bone ball was visually inspected to ensure its desired shape and characteristics. A disinfection process was then carried out, and finally, the prepared bone ball was appropriately stored until use in the equipment.

2.4 Wear

The wear test was conducted using the Nanovea T100 tribometer. In this test, a ball (bone) was in contact with a flat surface (uncoated alloy). Mechanical parameters were selected to simulate or slightly exceed real-world conditions, with an applied average load of 7N, a speed of 1.09 m/s (similar to walking speed), and a displacement of 6 mm

2.5 Corrosion and friction corrosion

For corrosion assessment, tests were conducted in triplicate using a Gamry potentiostat-galvanostat Interface 1000E model, applying electrochemical impedance spectroscopy (EIS) and Tafel polarization curves [29]. These experiments were carried out at 37 °C to simulate human body conditions using the previously specified solution [30]. The working cell configuration consisted of a standard three-electrode system [31], where a platinum electrode served as the counter electrode, an SCE electrode as the reference, and the [TiN/TiAlN] multilayer coating deposited on Ti6Al4V as the working electrode. The exposed surface area of the sample was 1 cm^2, and the system was allowed to reach a constant potential value for 90 minutes as a stabilization time. During the test, a potential sweep of 0.25 mV/s was performed in the -300-mV vs. OCP range to 300 mV vs OCP [32].

The Nanovea T 100 tribometer was employed for the friction corrosion test, incorporating the linear liquid bath module to conduct wear and friction experiments in liquid environments. After the sliding friction was stopped, the open circuit potential (OCP) was recorded for an additional 10 minutes to evaluate the repassivation behavior of the coating surface. The pure wear and tribocorrosion tests were conducted three times for each coating variant to ensure the robustness and reliability of the results [33][34]. This system was specifically utilized for friction and corrosion testing, where a ball (simulating bone) was in contact with a flat surface (uncoated alloy) submerged in the test fluid. Mechanical parameters were selected to mimic or slightly exceed real-world conditions, with an applied average load (P) of 7 N and a speed set to 1.09 m/s, akin to a person's walking speed. Additionally, a 6 mm displacement was applied. This methodology aligns with ASTM G119-09(2021) [35], which provides a standard guide for determining the synergism between wear and corrosion.

2.6 Characterization of multilayer coatings after wear testing

The multilayers were characterized using scanning electron microscopy (SEM) in a Philips XL 30 FEG at 15 keV to assess the effects of the wear test on their surface morphology. To obtain a more detailed view of the surface topography and understand how the coating affects the material's response to corrosion and friction processes at the microscopic level, further analysis was carried out using atomic force microscopy (AFM) in contact mode with a Si_3N_4 tip in a Nanosurf NaniteAFM.

3. RESULTS

3.1 XRD analysis of coatings

The X-ray diffraction (XRD) results for TiAlN coatings are presented in Figure 1, demonstrating that all coatings exhibit similar precipitated phases, including TiN, TiAlN, and AlN. The total measured thickness of the deposited $[TiN/AlTiN]_{24}$ multilayered coatings is approximately 3 µm. The individual layer thicknesses varied as a function of the bilayer number (24), resulting in a layered structure with individual thicknesses around 125 nm, corresponding to the bilayer period (Λ). Figure 1 shows the XRD pattern for TiN/AlTiN coatings deposited with Λ = 125 nm onto a Si (100) substrate under r.f. conditions. The XRD pattern displays characteristic peaks corresponding to diffractions from the TiN (111) at 35°, TiAlN (200) at 47°, and AlN (220) at 67.69° planes of the FCC structure. These preferential orientations align with the International Centre for Diffraction Data (ICDD) files ICSD 98-009-8009, ICSD 98-006-1166, and ICSD 98-008-0927. The pattern also reveals a cubic structure where the most intense peak (220) corresponds to the AlTiN (220) plane at 55.32°, suggesting a slightly textured growth along this orientation.

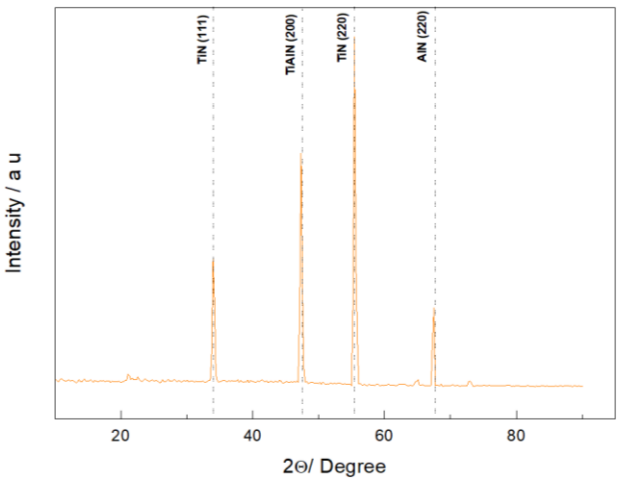

Fig. 1. X-ray diffraction (XRD) patterns of the TiN/AlTiN multilayer coatings with 24 bilayers. The dashed lines indicate the location of the identified peaks.

In the films, four crystalline planes of titanium aluminium nitride are identified. However, it is important to emphasise that the intensity peaks corresponding to these planes do not appear in all spectra of the multilayers. The first two, which correspond to the planes (111) and (220), had been previously identified during the deposition of the titanium nitride layer. In contrast, the TiAlN plane only manifests in the context of multilayers, highlighting its specific relevance in this type of structure.

Furthermore, the preferential orientation of the (200) plane is linked to the fact that multilayers will grow on those planes where the total energy is minimised. This total energy is the sum of the surface energies and strain energies. Thus, a competition is established between the different planes, whereby only the plane exhibiting the minimal values of these energies will be able to grow and become the preferential plane. This finding underscores the growth dynamics of the multilayers and their dependence on energetic conditions, which is fundamental for understanding the behaviour of these coatings in practical applications.

These findings are consistent with those reported by J. Chen et al. [36], In their work, the authors also observed a preferential texture in multilayered TiN/AlTiN coatings, confirmed by XRD analysis, like the textures described in the present study.
The Nelson- Riley extrapolation technique was employed for the lattice parameter determination, obtained from the preferential orientation in both TiN and TiAlN single-layered coatings and in the multilayered structure analyzed in this study [7]. This method was chosen for the refinement procedure as it precisely determines the lattice constant, providing a value of 0 (±0.0001 nm).

However, it is essential to address the accuracy of stoichiometric analysis as EDX techniques have limited reliability for measuring nitrogen concentration. To account for this, elemental concentrations obtained from EDX were corrected using the ZAF method. This correction is crucial due to matrix effects related to the atomic number (Z), absorption (A), and fluorescence (F) that can influence the X-ray spectrum during electron microprobe analysis. These factors must be adjusted to ensure precise results. Initially, the ZAF correction factors were established using a standard specimen with known compositions. Corrections for peak K intensity were made to address dead time effects and reference X-ray measurements. Prior to each quantitative EDX spectrum analysis, both manual background correction and automated ZAF correction were performed. The EDX values for TiNx and Ti1-xAlxNy single layers, deposited with an RF negative bias voltage of -70 V, are presented in Table 2.

Table 2. Stoichiometric relationship analyzed by EDX with subtractions of oxygen contribution and lattice parameter of TiN_x and $Ti_{1-x}Al_xN_y$ single layer coatings.

Negative r.f. bias voltage (V)	Binary coatings ($Ti_{1-x}N_x$)	a_0 (nm) FCC (111) ($Ti_{1-x}N_x$)	Ternary coatings ($Ti_{1-x}Al_xN_y$)	a_0 (nm) FCC (220) ($Ti_{1-x}Al_xN_y$)
-70	$Ti_{0.4}N_{0.6.}$	0.4240	$Ti_{0.14}Al_{0.15}N_{0.71}$	0.4175

3.2 Scanning Electron Microscopy (SEM)

In Figure 2, it is observed that the layers are almost parallel to the substrate, indicating a low degree of waviness in the superlattice. This near-parallel alignment suggests that during the growth of the coating, an intense ion bombardment occurred, significantly influencing the overall microstructure. Ion bombardment enhances atomic mobility, allowing surface atoms to rearrange more efficiently. Consequently, coatings subjected to higher levels of bombardment tend to exhibit smoother surfaces, significantly reduced grain sizes, and decreased porosity [7]. This increased mobility contributes to a minimisation of surface roughness, producing films with superior surface finishes and improved mechanical properties. Although the resolution of the SEM images is insufficient to determine whether individual layers exhibit a distinct columnar structure, it is anticipated that such columnar growth would be disrupted at the interfaces, especially as the multilayer period decreases. This disruption at the interfaces could potentially result in grain refinement, thereby affecting the mechanical and physical properties of the multilayers [17].

The modulation and microstructure of the TiN/TiAlN multilayers were further characterised using high-resolution scanning electron

microscopy (SEM) images, providing critical insights into the periodic arrangement and integrity of the multilayer stacks. Figure 2 presents a cross-sectional view of a TiN/TiAlN coating with n = 24, where each individual layer is distinguishable [12]. The darker contrast of the TiAlN layers, compared to the TiN layers, facilitated the clear identification of the layered structure. This difference in contrast is due to variations in atomic number and density between the two materials, which is commonly exploited in SEM to enhance contrast between different layers. The TiN/TiAlN coatings exhibited a well-defined and consistent periodicity, a key feature for achieving the desired mechanical and tribological properties in these coatings. The SEM images confirmed that the bilayer thicknesses, as well as the total coating thickness, were in close agreement with the pre-designed values, demonstrating that the deposition process was well-controlled.

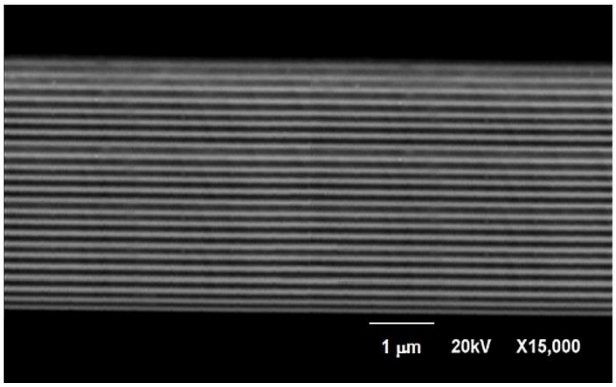

Fig. 2. Cross-sectional scanning electron microscopy image of a [TiN/TiAlN]n multilayer with n = 24 (left panel) and an enlarged view of the central section (right panel), showing details of the interface morphology.

However, the SEM images also revealed a slight deviation in the relative thicknesses of the nanometric layers. In this particular sample, the TiAlN layers appeared marginally thicker than the TiN layers, which may be attributed to subtle variations in the deposition parameters or differential growth rates between the two materials. Although minor, such deviations can significantly impact the overall properties of the coating, including its mechanical strength and wear resistance. The limited resolution of SEM when analysing interfaces at the nanometric scale presents challenges in accurately determining the thickness of each individual layer, particularly in the case of extremely thin multilayers. Nevertheless, the overall structural integrity of the multilayers remained intact.

Moreover, the SEM analysis provided insights into the effect of wavy interfaces on the strain incorporated into the TiN/TiAlN multilayer structure. In this study, it was observed that the TiN layers, which initially exhibited a flat morphology at the TiAlN/TiN interfaces, gradually evolved into a wavy morphology as additional material was deposited. This wavy structure could arise from stress relaxation mechanisms that occur during the deposition process, where strain accumulated at the interfaces between the TiAlN and TiN layers leads to undulations in the layer morphology. Interestingly, the TiAlN spacer layers appeared to mitigate the waviness, as they suppressed the undulations and restored a flatter morphology in the subsequent TiN layers. This suppression of waviness by the TiAlN layers could be attributed to their capacity to absorb and redistribute stress, thereby maintaining a more uniform and controlled layer structure [16].

In summary, the SEM analysis highlights the crucial role that ion bombardment, layer modulation, and interfacial effects play in determining the final microstructure of TiN/TiAlN multilayers. These factors not only affect the thickness and periodicity of the layers, but also significantly influence mechanical properties such as hardness, toughness, and wear resistance, making them key parameters in the design and optimisation of multilayer coatings.

3.3 Scratch test

The scratch testing technique was employed to characterise the adhesion resistance of the multilayer coating, providing valuable insights into the adhesive properties by determining the upper critical load (UCL) the threshold at which delamination initiates. This method is highly effective in evaluating how coatings respond to mechanical stress, offering a precise assessment of their performance in terms of wear resistance and failure mechanisms. Understanding these properties is essential, as poor adhesion can result in rapid wear, chipping, or catastrophic failure under operational conditions, which can severely compromise the reliability of components in industrial settings. Previous studies [37] have consistently emphasised the significance of adhesion strength as a key factor in the long-term durability of coated materials, particularly when subjected to extreme stress or abrasive environments.

As illustrated in Figure 3, the critical loads corresponding to adhesive failure for various coatings show that TiN/TiAlN multilayer coatings exhibit exceptional adhesion performance. This is particularly significant in industrial applications where coatings are exposed to high levels of wear, and their ability to remain adhered to the substrate is crucial for ensuring the longevity and reliability of the coated components. Inadequate adhesion, by contrast, can lead to early onset of delamination, increased wear rates, and ultimately, coating failure. Such failures not only diminish the functional properties of the coating but can also result in costly downtime or repairs in industrial processes [38]. The strong adhesion exhibited by these multilayer coatings underscores their suitability for use in demanding operational environments where reliability and performance are essential.

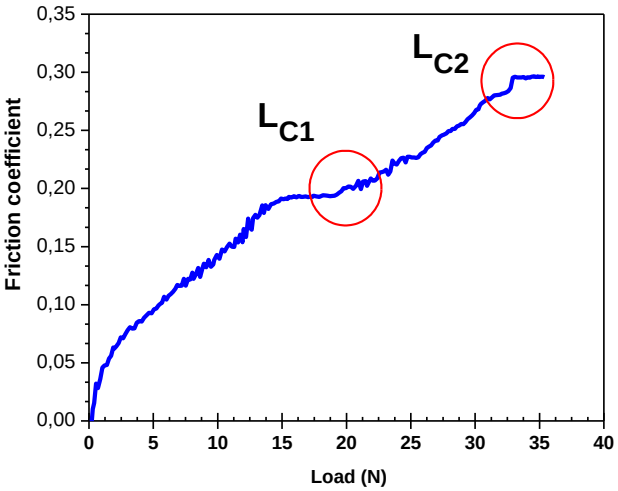

Fig. 3. Scratch test results for multilayer coating with n=24.

The coatings' resistance to adhesive failure under elevated loads can be largely attributed to the synergistic interactions between the individual layers within the multilayer system. These interactions, together with the high-quality interfaces formed during the deposition process, are key in enhancing the overall mechanical integrity of the coating. This has been corroborated by various studies, which show that the mechanical properties of multilayer coatings such as hardness, toughness, and resistance to crack propagation—are highly dependent on the microstructure of the layers and the quality of the interfaces between them [39]. The formation of strong, cohesive interfaces between layers ensures that the coating can distribute mechanical stress more effectively, reducing the likelihood of delamination, even under challenging conditions.

Notably, the multilayer system with n=24 layers demonstrated particularly robust performance under applied loads, further emphasising the critical role of mechanical strength and internal cohesion in multilayer coatings. This robustness is indicative of the optimised design of the coating architecture, where the strategic arrangement of layers contributes to an enhanced ability to withstand mechanical stresses. Such performance is particularly relevant for applications requiring high wear resistance and durability, as the mechanical strength of the coating directly influences its service life. Previous research has also highlighted the importance of optimising parameters such as layer thickness, material composition, and deposition conditions to enhance the performance of multilayer coatings. Studies have shown that by fine-tuning these factors, significant improvements can be made in terms of adhesion strength, resistance to cracking, and overall durability, especially under conditions that closely mimic real-world industrial applications [39].

In addition to the adhesion properties, this study provides valuable insights into the overall performance of the coatings in operational environments. The comprehensive understanding gained from these evaluations not only enhances the durability and effectiveness of coating in industrial applications but also lays the groundwork for future advancements in coating technology. By identifying the critical parameters that govern coating performance, researchers can continue to develop innovative solutions tailored to meet the ever-evolving demands of industries such as aerospace, automotive, and manufacturing, where high-performance coatings are indispensable.

Moreover, it is important to highlight that, to ensure a valid and fair comparison among the different coating systems studied, certain experimental conditions were rigorously controlled. Specifically, it was assumed that the adhesion between the substrate and the first layer of the multilayer system remained constant across all samples [40]. This assumption was based on the uniformity in the preparation and conditioning of the samples, as well as the consistent deposition parameters used throughout the study. These measures ensured that any observed variations in adhesion behavior were solely attributable to the intrinsic properties of the coating materials and the characteristics of the

interfaces between the individual layers within the multilayer system. Additionally, the parameters of the scratch test were kept consistent for all samples, ensuring that the results accurately reflect the relative performance of the coatings, independent of external test conditions. This meticulous approach guarantees that the conclusions drawn from the study are robust and reliable, offering meaningful insights into the design and application of advanced multilayer coating systems [41].

3.4 Corrosion and friction corrosion results

Figure 4 shows the potential behavior as a function of time for both the substrate and the coating under corrosion and friction-corrosion conditions. An increase in the corrosion potential (Ecorr) is observed for both the substrate and the coating when subjected to friction, indicating improved corrosion resistance due to the formation of corrosion products that act as a barrier. The coating, in particular, exhibits a significant increase in potential, reaching more positive values, which suggests greater chemical stability and protective capacity even under mechanical wear conditions. This behavior reflects the coated system's ability to resist degradation, maintaining a higher potential that indicates a lower tendency to corrode compared to the bare substrate.

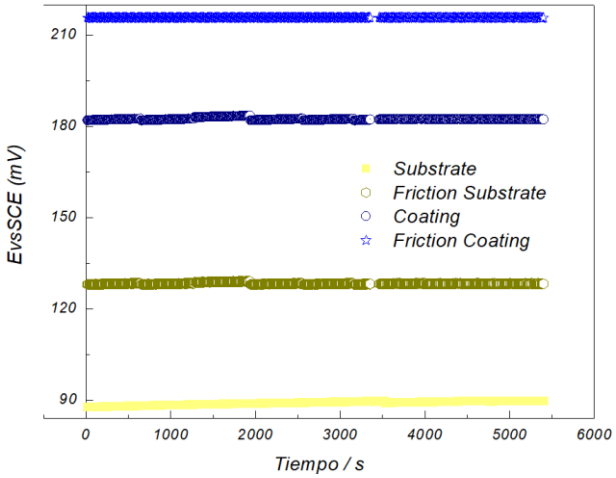

Fig. 4. Open circuit potential as a Function of Time for Substrate and Coating Under Corrosion and Friction-Corrosion Conditions.

Fig. 5 depicts the potentiodynamic polarisation tests carried out on both uncoated and coated substrates, each immersed separately in a simulated biological fluid solution. The corresponding mean values and standard deviations for corrosion potential (Ecorr), current density (Icorr), and corrosion rate (Rcorr) are summarised in Table 3. In this context, Ecorr indicates the tendency of the substrate to undergo corrosion, while Rcorr reflects the rate at which corrosion occurs [34]. The Icorr values were estimated by fitting linear Tafel extrapolations using Gamry Echem Analyst software, a well-established approach in electrochemical analysis.

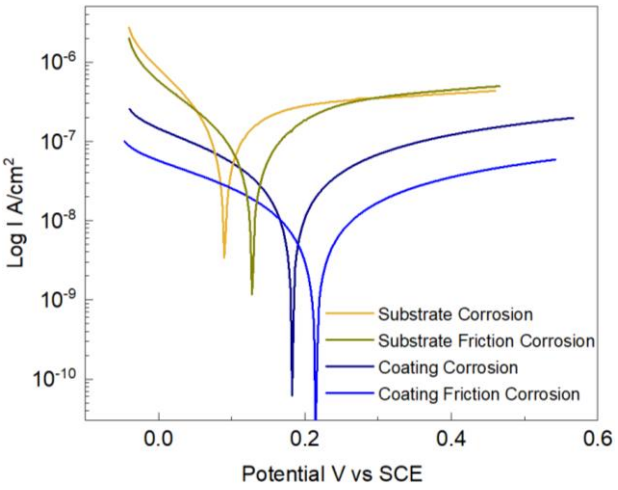

Fig. 5. Tafel polarization curves of Ti6Al4V substrates and $[TiN/TiAlN]_{24}$ coatings evaluated in corrosion and friction corrosion in simulated biological fluid at 37 °C.

Table 3. provides a comprehensive overview of the electrochemical behaviour of both the Ti6Al4V alloy substrate and coated surfaces, presenting key parameters such as Ecorr (corrosion potential), Icorr (corrosion current), and CR (corrosion rate).

Specimens	E_{Corr} (V vs SCE)	I_{Corr} (A/cm²)	Corrosion rate/ (μm·year⁻¹)
Corrosion Substrate	0.0897	1.03×10^{-7}	0.52
Corrosion Friction Substrate	0.1284	4.81×10^{-8}	0.242
Corrosion Coating	0.1828	1.80×10^{-8}	0.091
Corrosion Friction Coating	0.2151	5.02×10^{-9}	0.025

The results show that the Ecorr for the uncoated substrate under corrosion conditions was 0.089 V vs. SCE (Saturated Calomel Electrode), rising to 0.128 V vs. SCE in the combined corrosion-wear system. In contrast, the coated substrate exhibited

a corrosion potential of 0.1828 V vs. SCE under pure corrosion, with a further increase to 0.215 V vs. SCE when subjected to friction corrosion. This trend towards higher potentials for both coated and uncoated substrates, particularly in friction-corrosion systems, points to the accumulation of corrosion products in areas with low fluid circulation. This build-up can locally inhibit corrosion by creating a barrier, although it can also promote the release of metal ions from the worn surfaces, even in coated systems [38].

The observed shift towards more positive or cathodic potentials under friction corrosion is of particular thermodynamic importance. A higher corrosion potential typically signifies a greater level of chemical inertness, implying better corrosion resistance. In dual corrosion-wear systems, this phenomenon is associated with the formation of a passive film on the surface, which acts as a protective layer. In the case of the uncoated substrate, re-establishing this stable oxide layer—capable of protecting the surface—takes longer under wear conditions compared to pure corrosion, as mechanical forces constantly disrupt the oxide formation.

This protective behaviour is largely governed by the surface's response to deformation caused by wear. During sliding, passivation leads to the continuous reconstruction of the protective layer. This reconstructed layer plays a crucial role in limiting dislocation movement on the worn surface, which would otherwise result in extensive surface deformation. In the coated systems, this leads to less deformed worn surfaces and improved resistance to wear-induced corrosion.

Further insights into the effectiveness of the coatings can be drawn from the potentiodynamic curves, which show a pronounced downward shift along the current density axis for the coated substrates, positioning these curves significantly below those of the uncoated substrate. This shift indicates that the coatings possess a much lower corrosion current density, which correlates with superior corrosion resistance. Specifically, the coated systems demonstrate a markedly lower Icorr, signifying reduced metal dissolution. In particular, the coating's performance under friction-corrosion conditions stands out, with the $[TiN/TiAlN]_{24}$ system offering exceptional protection compared to the uncoated Ti6Al4V substrate.

Based on these observations, a clear performance ranking can be established, arranged according to decreasing corrosion density and rate: $[TiN/TiAlN]_{24}$ evaluated in friction corrosion > $[TiN/TiAlN]_{24}$ evaluated in corrosion > Ti6Al4V evaluated in friction corrosion > Ti6Al4V evaluated in corrosion. This hierarchy highlights the superior performance of the $[TiN/TiAlN]_{24}$ coating, particularly in environments that simultaneously impose corrosion and mechanical wear stresses. The enhanced performance is largely due to the multilayered structure of the $[TiN/TiAlN]_{24}$ coating, which promotes stronger adhesion, superior mechanical properties, and faster formation of a protective passive layer.

The analysis of densities and corrosion rates in our study has demonstrated a significant improvement in corrosion resistance provided by the thin film applied to the substrate. This enhancement is reflected in the increase in corrosion potential, the decrease in anodic current, and the reduction in Ti ion release. To contextualize our findings, it is crucial to compare these results with similar studies investigating coatings with analogous purposes.

When comparing our results with the study by Caicedo et al. [40], we find a notable agreement in observations regarding the anticorrosive protection of multilayer films. In their research, Caicedo et al [24]. investigated the effectiveness of TiN/TiAlN multilayer coatings and concluded that these films offer effective corrosion protection. Our findings support this conclusion, as we have also observed a significant improvement in corrosion resistance, similar to that reported in their study. This concordance underscores the robustness of TiN/TiAlN multilayer films in anticorrosive protection [41].

On the other hand, when comparing our results with the study by Subramanian et al. [42], we also find that TiN/TiAlN multilayer films present a face-centered cubic (FCC) structure with a partial arrangement of Ti and Al atoms. This study highlights that this structure significantly contributes to the anticorrosive capacity of the coatings. Moreover, the observation that blood platelets adhere differently to the coatings compared to bare titanium emphasizes the effectiveness of these coatings in biomedical applications. In our study, the thin films' ability to enhance corrosion resistance and their compatibility in biocompatibility tests reinforces these observations.

Moreover, the effectiveness of TiAlN coatings in reducing wear and corrosion aligns with findings from similar studies on other coatings, such as those conducted by Saravanan et al [43]. and Kumar et al [44]. These studies indicate that while TiN and other coatings also offer good performance, the ability of TiAlN to maintain its properties under diverse conditions and mitigate wear more effectively distinguishes it. This makes TiAlN coatings particularly suitable for applications in aggressive environments, including biomedical fields, where durability and reliability are paramount.

When an increase in corrosion potential (ECorr) is observed for both the substrate and the coating under friction-corrosion conditions, it is essential to note that this rise is primarily due to the formation of corrosion products, which act as temporary passive barriers. The chemical stability exhibited by the coating is crucial, as it suggests that these corrosion products not only halt further degradation but also protect the coating's surface from additional wear, thereby extending its lifespan. However, this protection may not be permanent if the corrosion products detach or if the protective film weakens over time due to repeated cycles of friction and corrosion.
It is particularly important to consider how the interaction between corrosion and friction affects the coating's adhesion to the substrate. Much of the literature emphasises that an effective coating under these conditions must exhibit good internal cohesion and a strong interface with the substrate (V. Terek et al., 2024) [38]. This is because friction tends to exacerbate weaknesses in adhesion, which could lead to premature delamination of the coating. In this context, it is advisable to reference previous studies that have examined delamination resistance in multilayer systems under conditions of corrosion and friction, as these dynamics can significantly influence the overall performance of the system.

3.5 Wear rate

Fig 6 graphically presents the friction coefficient profiles for both the multilayer $[TiN/TiAlN]_{24}$ coating and the Ti6Al4V substrate. Friction coefficients were measured under identical testing conditions, with average values of 0.053 for the coating and 0.273 for the substrate, respectively. These results demonstrate a significant reduction in the friction coefficient for the multilayer coating, highlighting its effectiveness in mitigating frictional forces during operation.

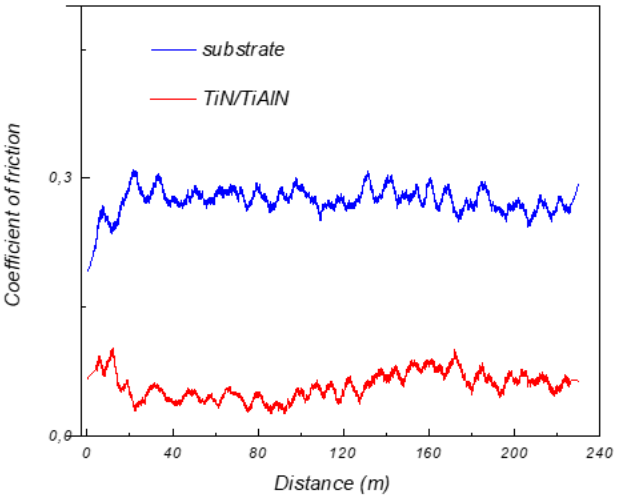

Fig. 6. The coefficient of friction profile is presented in detail for both the uncoated system and the multilayer coatings at a constant sliding speed of 1.09 m/s, applying a load of 7 N.

When considering the applied load and sliding speed, it is important to note that these results indicate discrete frictional behaviour in both specimens. However, the substantial 80.5% reduction in friction for the $[TiN/TiAlN]_{24}$ coating is particularly striking. This considerable decrease directly correlates with enhanced wear resistance, as lower friction generally results in less mechanical degradation of the contacting surfaces over time. The ability of the thin film to maintain such a low friction coefficient under stress underscores its superior tribological properties and emphasises its potential for applications where minimising energy loss due to friction is essential.

The observed reduction in the friction coefficient also suggests that the multilayer structure effectively distributes mechanical loads across its various layers, thereby reducing the concentration of wear at any single point of contact. This layered configuration likely contributes to the coating's ability to endure more severe wear conditions, consequently extending the operational lifespan of the coated component. Furthermore, the smoother surface finish of the coating (as corroborated by the AFM data) supports this reduction in friction, as fewer surface asperities are available to interact, resulting in lower resistance during sliding contact.

When compared to the uncoated Ti6Al4V substrate, the higher friction coefficient observed in the substrate can be attributed to its rougher surface, which increases asperity interactions and promotes higher wear rates. This finding is consistent with previous studies showing that uncoated titanium alloys typically suffer from higher friction and more rapid material loss in tribological systems. Furthermore, the wear rates for the pin in contact with the multilayer coating and the Ti6Al4V substrate were calculated. For the multilayer coating, the wear rate was found to be 9.6×10^{-7} $mm^3N^{-1}m^{-1}$, while for the substrate, it was 1.6×10−6 $mm^3N^{-1}m^{-1}$. This indicates that the multilayer coating exhibits significantly lower wear, translating to enhanced durability and performance.

In the study by Li et al. [45] on TiAlN/WS self-lubricating composite coatings, significant advancements in tool performance are demonstrated due to the low coefficient of friction (COF) and high adhesion of these coatings. Their results highlight a notable reduction in flank wear and an increase in cutting speed compared to TiAlN coatings alone, with the TiAlN/WS coatings showing superior performance in both dry and wet cutting conditions.

In contrast, the findings of your study, which focus on the impact of radio-frequency (RF) power on the structural and mechanical properties of N-Ni films, can be critically assessed by comparing these results with those presented in the Li et al [45]. For instance, while the TiAlN/WS coatings achieved a COF reduction from 1.507 to 0.261, indicating a significant improvement in self-lubricating properties, your study could benefit from a more detailed comparison of how varying RF power affects the COF and wear resistance of N-Ni films in contrast to these composite coatings. Additionally, addressing the mechanical performance of these coatings, particularly hardness and adhesion properties, in relation to your findings would provide a more comprehensive understanding of how different coating technologies compare in terms of practical applications and performance in challenging environments.

The effect of a coating's mechanical properties, such as its wear resistance, plays a crucial role in its ability to withstand friction-corrosion. The hardness of the coating not only impacts its scratch resistance but also determines how it responds to applied loads during contact with other materials. This is particularly vital in industrial environments where wear and corrosion occur synergistically. It is important to highlight that multilayer coating systems, such as TiAlN/TiN, often demonstrate better performance under such conditions due to the stress distribution between the layers. This layered structure allows for enhanced durability and resilience, mitigating the detrimental effects of combined mechanical and corrosive stresses.

3.6 SEM

As shown in Fig. 7, calculations based on microscopy images were performed to assess the volume loss of the spherical bone pin during corrosion-wear tests, following the guidelines outlined by ASTM G-99. This method allows for the accurate quantification of volume losses experienced by the bone pin under varying test conditions, providing valuable insights into the interaction between the bone-like material and different surfaces. The volume loss data helps to establish a direct link between the tribological performance of the tested materials and their ability to mitigate the wear of bone-like substrates under simulated conditions.

For the pin in contact with the coated surface (Fig. 7b), a significantly lower volume loss of 0.001606 mm^3 was observed, indicating that the coating provides substantial protection against material removal. In contrast, when the pin interacted with the uncoated substrate (Fig. 7a), a notably higher volume loss of 0.00260 mm^3 was recorded, suggesting that, in the absence of a protective coating, a greater amount of bone-like material is detached. These results clearly highlight the protective role of the coating, as it minimises material removal and prevents excessive wear of the bone-like substrate. The observed volume loss in the uncoated system indicates that more aggressive mechanical action occurs, likely due to the higher surface roughness and the absence of a passive layer that would otherwise provide a barrier against wear and corrosion.

The tribological behaviour observed is consistent with findings from the friction coefficient data (Fig. 6), which further corroborates the protective effects of the coating. Once movement is initiated

in the uncoated system, a considerable amount of bone is removed through abrasion, which in turn alters the surface roughness and significantly affects the frictional response. This dynamic interaction between the substrate and the bone material initiates a cyclical process, where continuous detachment and transfer of bone-like material occur, resulting in fluctuating friction behaviour. As the wear progresses, some of the detached bone adheres to the substrate, leading to repeated cycles of contact that further influence the friction coefficient. The test results suggest that this pattern continues throughout the 230-meter duration of the experiment, with the volume loss and friction cycles reinforcing each other.

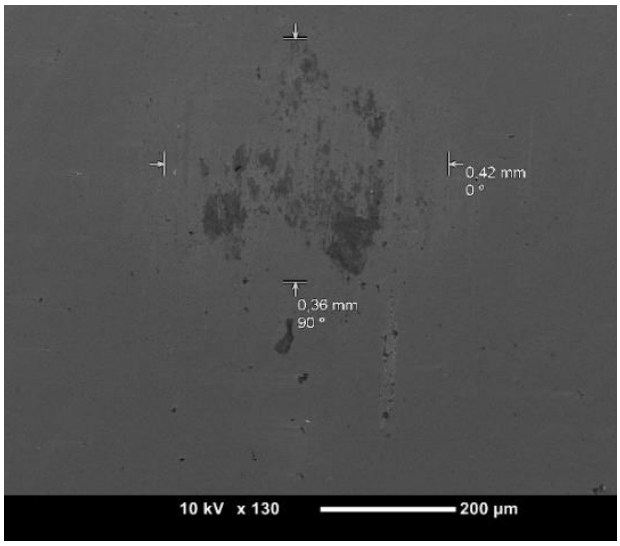

(a)

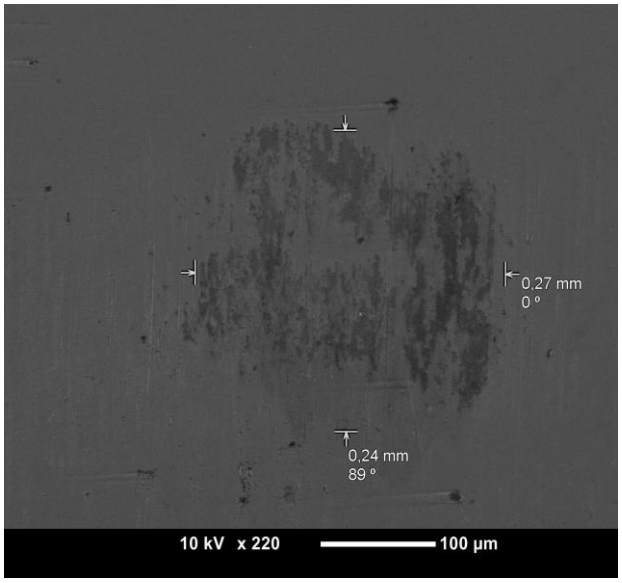

(b)

Fig. 7. Microscopy images of the surface of the pin: a) uncoated specimens, b) coated specimens, after tribology test.

In contrast, the coated system exhibits a markedly different wear profile. The initial bone wear in contact with the coated surface is significantly lower, which can be attributed to the smoother surface finish of the coating. The lower roughness reduces the potential for abrasive wear, and as a result, the bone material is not as severely affected. Moreover, the bone does not adhere as strongly to the coated surface, making it easier for the material to detach and preventing the formation of wear particles that could otherwise lead to more severe damage. This behaviour suggests that the coating provides an effective barrier, not only protecting the underlying material but also minimising the wear of the bone-like substrate.

Interestingly, when comparing these tribological results with the findings from electrochemical tests, it becomes evident that bone wear correlates with the removal of the passive layer from the surface. During the corrosion-wear process, the active removal of the passive layer in the uncoated system results in a higher material loss, particularly in the active zone where corrosion is more aggressive. This active zone is characterised by a combination of mechanical wear and electrochemical corrosion, which accelerates the degradation of the uncoated substrate. In the case of the coated system, the passive layer is more stable, preventing significant material loss and ensuring better overall performance in terms of both wear and corrosion resistance.

3.7 AFM

The atomic force microscopy (AFM) images in Figures 8a and 8b provide a detailed view of the surfaces before undergoing wear. In the first image, the Ti6Al4V substrate exhibits an initial roughness of 45.92 µm, a relatively high value that indicates a coarse surface finish, which could adversely affect its performance in tribological applications. In contrast, the $[TiN/TiAlN]_{24}$ coating, shown in Figure 8b, displays a significantly lower roughness of 0.4882 µm, indicative of a smoother and more uniform surface characteristic of thin-film coatings. Such smoothness is essential for minimising friction and wear, particularly in high-stress environments, as it reduces the interaction between surface asperities, which are often the points of mechanical failure.

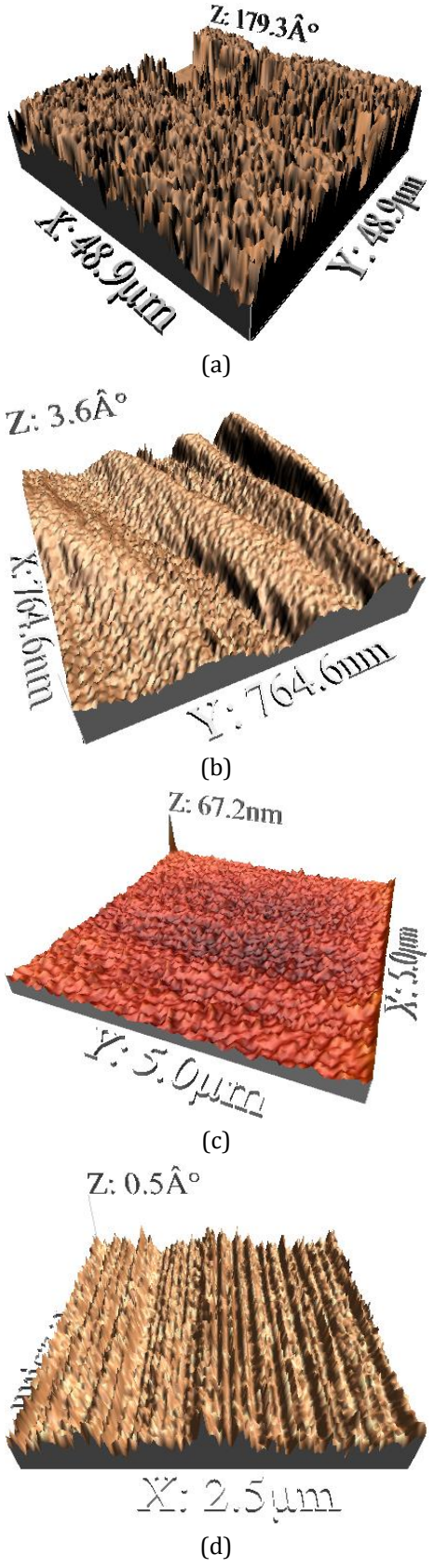

Fig. 8. Displays atomic force microscopy (AFM) images depicting the following conditions: the uncoated surface (Fig. 8a), the surface coated with multiple layers (Fig. 8b), the substrate after undergoing corrosion-friction (Fig. 8c), and the coating surface post-exposure to corrosion-friction (Fig. 8d).

Further examination of Figures 8c and 8d reveals the conditions after wear. In Figure 8c, the worn Ti6Al4V substrate shows a decrease in surface roughness (Ra) to 0.3864 µm, suggesting that the surface has undergone substantial wear, leading to a smoother profile compared to its initial state. However, this reduction in roughness should not be interpreted as an improvement in performance; rather, it indicates that the material has been worn down and abraded during the test. This wear-induced smoothing can be detrimental, as it compromises the structural integrity of the material, making it more vulnerable to further damage under continued mechanical loading.

In sharp contrast, the $[TiN/TiAlN]_{24}$ coating, even after wear, retains an impressively smooth surface with a roughness of just 0.0482 µm (Figure 8d). This minimal change in surface topography suggests that the coating experiences only superficial damage, in line with expectations that such multilayer coatings offer superior resistance to wear and corrosion. The coating's ability to preserve its structural integrity despite frictional forces highlights its protective function, indicating that the multilayer structure effectively distributes stress across its layers, thereby preventing significant surface degradation.

The comparison of roughness values before and after wear provides a quantitative measure of surface alteration. While the Ti6Al4V substrate shows a decrease in roughness, it also undergoes considerable material removal, which signifies poor tribological performance compared to the coated sample. Conversely, the $[TiN/TiAlN]_{24}$ coating's ability to maintain low roughness after wear underscores its exceptional performance in preserving surface quality under challenging conditions. This capability is critical for extending the lifespan of materials exposed to friction and wear, especially in industrial environments where surface degradation can lead to premature failure.

The AFM analysis further corroborates the superior wear resistance of the multilayer coating. The smooth surface observed after wear suggests moderate friction levels, as rougher surfaces typically increase friction due to greater asperity interaction. By maintaining its smoothness, the $[TiN/TiAlN]_{24}$ coating reduces frictional forces, resulting in lower energy dissipation and enhanced efficiency in

mechanical systems. This not only improves the durability of the coated material but also reduces the frequency of maintenance and part replacement in industrial applications [46].

The AFM images also revealed a more extensively deformed microstructure on the worn surface of the Ti6Al4V substrate in samples tested solely under the influence of corrosion. This observation indicates significant damage caused by corrosion in the absence of the protective multilayer coating. The deformation in these samples suggests that the substrate surface is more prone to wear in corrosive environments, likely due to the absence of a passivation layer that could shield the surface from aggressive chemical attack.

In contrast, the $[TiN/TiAlN]_{24}$ coating benefits from the formation of a passive layer during the corrosion-wear process, which acts as the primary mechanism for its protective properties. This layer effectively shields the underlying material from both chemical corrosion and mechanical wear, thereby slowing the rate of material degradation. The development of such a passive layer is crucial for extending the service life of coatings in harsh environments, where the combined effects of corrosion and wear can quickly compromise unprotected surfaces [47].

The AFM results, when combined with findings from electrochemical and tribological tests, clearly demonstrate the critical role that surface roughness plays in the wear resistance of coatings. A smoother surface lowers the likelihood of wear initiation, while the formation of a protective passive layer during corrosion-wear conditions further enhances the coating's durability. These findings emphasise the importance of optimising surface properties in the development of advanced coatings for industrial applications, particularly those involving complex interactions between mechanical and corrosive stresses.

4. CONCLUSION

The conclusions of this study underscore the significant advantages of TiAlN coatings compared to other commonly used types of coatings. One of the primary benefits of TiAlN coatings is their superior corrosion resistance, as evidenced by potentiodynamic polarization tests. These tests revealed a substantial shift in polarization curves and a marked reduction in corrosion density, directly resulting from the formation of TiN, TiAlN, and AlN phases in the coating. These phases align with previous research and exhibit preferred orientations that enhance the protective capabilities of the coating against corrosive environments.

In addition to corrosion resistance, TiAlN coatings also excel in wear resistance. Atomic force microscopy (AFM) analysis demonstrated that these coatings effectively reduce wear-induced deformation, further validating their robustness under challenging conditions. The coatings were particularly effective in minimizing material removal, as indicated by the significant reduction in volume loss observed in coated bone pins during corrosion-wear tests. This reduction in wear highlights the coating's ability to maintain structural integrity and performance over extended periods of use.

Compared to other coatings such as TiN, AlCrN, and DLC, TiAlN coatings exhibit distinctive advantages. For example, while TiN coatings show optimal wear resistance at specific sliding velocities and applied loads, TiAlN coatings provide improved performance over a wider range of conditions. Similarly, although AlCrN coatings are effective, they require different tribological parameters for optimal performance compared to TiAlN. The comprehensive optimization of TiAlN coatings, as demonstrated in this study, reveals that they offer superior performance by adapting to various operational conditions, unlike other coatings that may have more restricted optimal parameter ranges.

REFERENCES

[1] M. Oprea and S. I. Voicu, “Recent advances in composites based on cellulose derivatives for biomedical applications,” *Carbohydrate Polymers*, vol. 247, p. 116683, Jun. 2020, doi: 10.1016/j.carbpol.2020.116683.

[2] J. Quinn, R. McFadden, C.-W. Chan, and L. Carson, “Titanium for Orthopedic applications: An overview of surface modification to improve biocompatibility and prevent bacterial biofilm formation,” *iScience*, vol. 23, no. 11, p. 101745, Oct. 2020, doi: 10.1016/j.isci.2020.101745.

[3] S. Chowdhury and N. Arunachalam, "Surface functionalization of additively manufactured titanium alloy for orthopaedic implant applications," *Journal of Manufacturing Processes*, vol. 102, pp. 387–405, Jul. 2023, doi: 10.1016/j.jmapro.2023.07.015.

[4] A. Heidarzadeh *et al.*, "Friction stir welding/processing of metals and alloys: A comprehensive review on microstructural evolution," *Progress in Materials Science*, vol. 117, p. 100752, Oct. 2020, doi: 10.1016/j.pmatsci.2020.100752.

[5] X. Meng, Y. Huang, J. Cao, J. Shen, and J. F. D. Santos, "Recent progress on control strategies for inherent issues in friction stir welding," *Progress in Materials Science*, vol. 115, p. 100706, Jun. 2020, doi: 10.1016/j.pmatsci.2020.100706.

[6] Mohd. Z. B. Abdullah, M. A. Ahmad, A. N. Abdullah, M. H. Othman, P. Hussain, and A. Zainuddin, "Metal release of multilayer coatings by physical vapour deposition (PVD)," *Procedia Engineering*, vol. 148, pp. 254–260, Jan. 2016, doi: 10.1016/j.proeng.2016.06.612.

[7] A. Baptista, F. Silva, J. Porteiro, J. Míguez, and G. Pinto, "Sputtering Physical Vapour Deposition (PVD) Coatings: A Critical Review on Process improvement and Market Trend Demands," *Coatings*, vol. 8, no. 11, p. 402, Nov. 2018, doi: 10.3390/coatings8110402.

[8] S. Rashid *et al.*, "Biocompatibility and antibacterial properties of TiCu(Ag) thin films produced by physical vapor deposition magnetron sputtering," *Applied Surface Science*, vol. 573, p. 151604, Oct. 2021, doi: 10.1016/j.apsusc.2021.151604.

[9] D. Kışla *et al.*, "Recent developments in antimicrobial surface coatings: Various deposition techniques with nanosized particles, their application and environmental concerns," *Trends in Food Science & Technology*, vol. 135, pp. 144–172, Mar. 2023, doi: 10.1016/j.tifs.2023.03.019.

[10] M. Sathish, N. Radhika, and B. Saleh, "A critical review on functionally graded coatings: Methods, properties, and challenges," *Composites Part B Engineering*, vol. 225, p. 109278, Sep. 2021, doi: 10.1016/j.compositesb.2021.109278.

[11] R. A. De Jesus *et al.*, "Metal/metal oxide nanoparticles: A revolution in the biosynthesis and medical applications," *Nano-Structures & Nano-Objects*, vol. 37, p. 101071, Nov. 2023, doi: 10.1016/j.nanoso.2023.101071.

[12] A. Ghorbani, H. Elmkhah, O. Imantalab, M. Meghdari, M. Nouri, and A. Fattah-Alhosseini, "The impact of mechanical post-treatment on the tribological and corrosion behavior of CrN/CrAlN coatings applied using the CAE-PVD technique," *Applied Surface Science Advances*, vol. 18, p. 100477, Oct. 2023, doi: 10.1016/j.apsadv.2023.100477.

[13] N. M. Rafiq, W. Wang, S. L. Liew, C. S. Chua, and S. Wang, "A review on multifunctional bioceramic coatings in hip implants for osteointegration enhancement," *Applied Surface Science Advances*, vol. 13, p. 100353, Dec. 2022, doi: 10.1016/j.apsadv.2022.100353.

[14] A. Kumar and R. S. Mulik, "Improving tribological behavior of titanium nitride (TiN) hard coatings via zirconium (Zr) or vanadium (V) doping," *Tribology International*, vol. 189, p. 108997, Oct. 2023, doi: 10.1016/j.triboint.2023.108997.

[15] A. Roy, P. Patel, N. Sharifi, R. R. Chromik, P. Stoyanov, and C. Moreau, "Binary and ternary lubricious oxides for high temperature tribological applications: A review," *Results in Surfaces and Interfaces*, vol. 11, p. 100117, May 2023, doi: 10.1016/j.rsurfi.2023.100117.

[16] L. Sheng *et al.*, "Influence of layer number on microstructure, mechanical properties and wear behavior of the TiN/Ti multilayer coatings fabricated by high-power magnetron sputtering deposition," *Journal of Manufacturing Processes*, vol. 70, pp. 529–542, Sep. 2021, doi: 10.1016/j.jmapro.2021.09.002.

[17] H.-S. Cao *et al.*, "Effect of bias voltage on microstructure, mechanical and tribological properties of TiAlN coatings," *Transactions of Nonferrous Metals Society of China*, vol. 32, no. 11, pp. 3596–3609, Nov. 2022, doi: 10.1016/s1003-6326(22)66042-4.

[18] A. R. Khan, N. S. Grewal, C. Zhou, K. Yuan, H.-J. Zhang, and Z. Jun, "Recent advances in biodegradable metals for implant applications: Exploring in vivo and in vitro responses," *Results in Engineering*, vol. 20, p. 101526, Oct. 2023, doi: 10.1016/j.rineng.2023.101526.

[19] M. Aliofkhazraei *et al.*, "Review of plasma electrolytic oxidation of titanium substrates: Mechanism, properties, applications and limitations," *Applied Surface Science Advances*, vol. 5, p. 100121, Jul. 2021, doi: 10.1016/j.apsadv.2021.100121.

[20] D. Royhman *et al.*, "Fretting-corrosion in hip taper modular junctions: The influence of topography and pH levels – An in-vitro study," *Journal of the Mechanical Behavior of Biomedical Materials/Journal of Mechanical Behavior of Biomedical Materials*, vol. 118, p. 104443, Mar. 2021, doi: 10.1016/j.jmbbm.2021.104443.

[21] S. Barril, N. Debaud, S. Mischler, and D. Landolt, "A tribo-electrochemical apparatus for in vitro investigation of fretting–corrosion of metallic implant materials," *Wear*, vol. 252, no. 9–10, pp. 744–754, May 2002, doi: 10.1016/s0043-1648(02)00027-3.

[22] H. Benzouid *et al.*, "Examining the microstructure, morphological features, and wetting characteristics of Ti/TiN/TiAlN thin films produced through RF/DC magnetron co-sputtering," *Materials Today Communications*, vol. 37, p. 107405, Oct. 2023, doi: 10.1016/j.mtcomm.2023.107405.

[23] L. Sheng *et al.*, "Influence of layer number on microstructure, mechanical properties and wear behavior of the TiN/Ti multilayer coatings fabricated by high-power magnetron sputtering deposition," *Journal of Manufacturing Processes*, vol. 70, pp. 529–542, Sep. 2021, doi: 10.1016/j.jmapro.2021.09.002.

[24] J. C. Caicedo, G. Cabrera, H. H. Caicedo, C. Amaya, and W. Aperador, "Nature in corrosion–erosion surface for [TiN/TiAlN]n nanometric multilayers growth on AISI 1045 steel," *Thin Solid Films*, vol. 520, no. 13, pp. 4350–4361, Feb. 2012, doi: 10.1016/j.tsf.2012.02.061.

[25] O. Mbanga, E. Cukrowska, and M. Gulumian, "Dissolution kinetics of silver nanoparticles: Behaviour in simulated biological fluids and synthetic environmental media," *Toxicology Reports*, vol. 9, pp. 788–796, Jan. 2022, doi: 10.1016/j.toxrep.2022.03.044.

[26] W. Aperador-Chaparro, J. H. Bautista-Ruiz, and A. S. Mejía, "Determinación por Visión Artificial del Factor de Degradación en Aleaciones Biocompatibles," *InformacióN TecnolóGica*, vol. 24, no. 2, pp. 109–120, Jan. 2013, doi: 10.4067/s0718-07642013000200012.

[27] D. M. G. Boggione, I. J. B. Santos, S. M. De Souza, and R. C. S. Mendonça, "Preparation of polyvinyl alcohol hydrogel containing bacteriophage and its evaluation for potential use in the healing of skin wounds," *Journal of Drug Delivery Science and Technology*, vol. 63, p. 102484, Mar. 2021, doi: 10.1016/j.jddst.2021.102484.

[28] O. B. Istanbullu and G. Akdogan, "Increased body fluid repellency and electrochemical corrosion resistance of intravascular stent materials by ICP-CVD-based DLC thin-film deposition," *Diamond and Related Materials*, vol. 138, p. 110251, Jul. 2023, doi: 10.1016/j.diamond.2023.110251.

[29] Y. Fu, F. Zhou, Q. Wang, M. Zhang, and Z. Zhou, "Electrochemical and tribocorrosion performances of CrMoSiCN coating on Ti-6Al-4V titanium alloy in artificial seawater," *Corrosion Science*, vol. 165, p. 108385, Dec. 2019, doi: 10.1016/j.corsci.2019.108385.

[30] Y. Liu, Y. Yang, X. Liu, J. Zheng, and S. Zhang, "Tribocorrosion of CrN coatings on different steel substrates," *Surface and Coatings Technology*, vol. 484, p. 130829, May 2024, doi: 10.1016/j.surfcoat.2024.130829.

[31] X. Hou *et al.*, "A systematic study of mechanical properties, corrosion behavior and biocompatibility of AZ31B Mg alloy after ultrasonic nanocrystal surface modification," *Materials Science and Engineering C*, vol. 78, pp. 1061–1071, Apr. 2017, doi: 10.1016/j.msec.2017.04.128.

[32] Y. Fu, F. Zhou, M. Zhang, Q. Wang, and Z. Zhou, "Structure and tribocorrosion behavior of CrMoSiCN nanocomposite coating with low C content in artificial seawater," *Friction*, vol. 9, no. 6, pp. 1599–1615, Nov. 2020, doi: 10.1007/s40544-020-0445-5.

[33] I. Milošev, "Corrosion inhibition of aluminium alloys by molybdate ions: A critical review of the chemistry, mechanisms and applications," *Corrosion Science*, vol. 229, p. 111854, Jan. 2024, doi: 10.1016/j.corsci.2024.111854.

[34] F. Zhou, J. Qian, M. Zhang, Y. Wu, Q. Wang, and Z. Zhou, "Tribocorrosion properties of CrMoN/Ag coatings with various Ag contents in seawater," *Surface and Coatings Technology*, vol. 473, p. 129993, Sep. 2023, doi: 10.1016/j.surfcoat.2023.129993.

[35] *Standard Guide for Determining Synergism Between Wear and Corrosion*, ASTM G119-09(2021), Jun. 2021.

[36] J. Chen, H. Li, and B. D. Beake, "Load sensitivity in repetitive nano-impact testing of TiN and AlTiN coatings," *Surface and Coatings Technology*, vol. 308, pp. 289-297, Dec. 2016, doi: 10.1016/j.surfcoat.2016.05.094.

[37] C. Mou, Z. Liu, G. Zhu, G. Zhang, and X. Cao, "Study on impact wear and damage mechanisms of DLC films on TC4 and 9Cr18 alloys," *Diamond and Related Materials*, vol. 148, p. 111390, Jul. 2024, doi: 10.1016/j.diamond.2024.111390.

[38] V. Terek *et al.*, "High-temperature tribological behavior of nanolayered TiAlN/TiSiN coating deposited on WC-Co cemented carbide," *Surface and Coatings Technology*, vol. 477, p. 130316, Dec. 2023, doi: 10.1016/j.surfcoat.2023.130316.

[39] V. F. C. Sousa, F. J. G. Da Silva, G. F. Pinto, A. Baptista, and R. Alexandre, "Characteristics and wear Mechanisms of TIALN-Based Coatings for Machining Applications: A Comprehensive review," *Metals*, vol. 11, no. 2, p. 260, Feb. 2021, doi: 10.3390/met11020260.

[40] J. C. Caicedo, G. Cabrera, W. Aperador, C. Escobar, and C. Amaya, "Corrosion-Erosion effect on TIN/TIALN multilayers," *Journal of Materials Engineering and Performance*, vol. 21, no. 9, pp. 1949–1955, Dec. 2011, doi: 10.1007/s11665-011-0093-z.

[41] W. Y. H. Liew, J. L. L. Jie, L. Y. Yan, J. Dayou, C. S. Sipaut, and M. F. B. Madlan, "Frictional and wear behaviour of ALCRN, TIN, TIALN single-layer coatings, and TIALN/ALCRN, ALN/TIN nano-multilayer coatings in dry sliding," *Procedia Engineering*, vol. 68, pp. 512–517, Jan. 2013, doi: 10.1016/j.proeng.2013.12.214.

[42] B. Subramanian, C. V. Muraleedharan, R. Ananthakumar, and M. Jayachandran, "A comparative study of titanium nitride (TiN), titanium oxy nitride (TiON) and titanium aluminum nitride (TiAlN), as surface coatings for bio implants," *Surface and Coatings Technology*, vol. 205, no. 21–22, pp. 5014–5020, May 2011, doi: 10.1016/j.surfcoat.2011.05.004.

[43] I. Saravanan, A. E. Perumal, R. F. Issac, S. C. Vettivel, and A. Devaraju, "Optimization of wear parameters and their relative effects on TiN coated surface against Ti6Al4V alloy," *Materials & Design*, vol. 92, pp. 23–35, Dec. 2015, doi: 10.1016/j.matdes.2015.11.119.

[44] S. Kumar, S. R. Maity, and L. Patnaik, "Morphology and wear behavior of monolayer TIALN and composite ALCRN/TIALN-Coated Plasma-Nitrided DAC-10 Tool Steel," *Arabian Journal for Science and Engineering*, vol. 47, no. 12, pp. 15519–15538, Mar. 2022, doi: 10.1007/s13369-022-06711-x.

[45] G. Li, W. Lü, S. Liu, C. Li, Y. Zhou, and Q. Wang, "Multilayer-growth of TiAlN/WS self-lubricating composite coatings with high adhesion and their cutting performance on titanium alloy," *Composites Part B Engineering*, vol. 211, p. 108620, Jan. 2021, doi: 10.1016/j.compositesb.2021.108620.

[46] C. Wang *et al.*, "Tribological behavior of Ti-6Al-4V against cortical bone in different biolubricants," *Journal of the Mechanical Behavior of Biomedical Materials/Journal of Mechanical Behavior of Biomedical Materials*, vol. 90, pp. 460–471, Oct. 2018, doi: 10.1016/j.jmbbm.2018.10.031.

[47] L. Patnaik, S. R. Maity, and S. Kumar, "Modeling of wear parameters and multi-criteria optimization by Box-Behnken design of AlCrN thin film against gamma-irradiated Ti6Al4V counterbody," *Ceramics International*, vol. 47, no. 14, pp. 20494–20511, Apr. 2021, doi: 10.1016/j.ceramint.2021.04.059.